Two-Step Phase Transition in SnSe and the Origins of its High Power Factor from First Principles

Antoine Dewandre,[1] Olle Hellman,[2,3] Sandip Bhattacharya,[4] Aldo H. Romero,[5,6] Georg K. H. Madsen,[7] and Matthieu J. Verstraete[1]

[1]*CESAM, QMAT, European Theoretical Spectroscopy Facility, Université de Liège, allée du 6 août, 19, B-4000 Liège, Belgium*
[2]*Division of Engineering and Applied Science, California Institute of Technology, Pasadena, California 91125, USA*
[3]*Department of Physics, Chemistry and Biology (IFM), Linköping University, SE-581 83 Linköping, Sweden*
[4]*ICAMS, Ruhr-Universität Bochum, 44780 Bochum, Germany*
[5]*Department of Physics, West Virginia University, 207 White Hall, 26506 West Virginia, USA*
[6]*Facultad de Ingenieria, Benemerita Universidad Autonoma de Puebla, 72570 Puebla, Pue., Mexico*
[7]*Institute of Materials Chemistry, TU Wien, A-1060 Vienna, Austria*

(Received 5 January 2016; revised manuscript received 25 August 2016; published 30 December 2016)

The interest in improving the thermoelectric response of bulk materials has received a boost after it has been recognized that layered materials, in particular SnSe, show a very large thermoelectric figure of merit. This result has received great attention while it is now possible to conceive other similar materials or experimental methods to improve this value. Before we can now think of engineering this material it is important we understand the basic mechanism that explains this unusual behavior, where very low thermal conductivity and a high thermopower result from a delicate balance between the crystal and electronic structure. In this Letter, we present a complete temperature evolution of the Seebeck coefficient as the material undergoes a soft crystal transformation and its consequences on other properties within SnSe by means of first-principles calculations. Our results are able to explain the full range of considered experimental temperatures.

DOI: 10.1103/PhysRevLett.117.276601

Thermoelectric (TE) materials and the thermoelectric effect are an interesting alternative energy source, harvesting waste heat from power production and other thermal engines. Despite their vast potential impact, only few materials are used in practice: most thermoelectric materials are highly toxic, expensive, and the devices present too low efficiencies to compete with other forms of power generation in industry. The main concern in this field is to discover or design thermoelectric materials that deal with these issues. The efficiency of a TE material is quantified by the thermoelectric figure of merit $zT = S^2\sigma T/(\kappa_{\mathrm{el}} + \kappa_l)$, which is the ratio of the electrical conductivity (σ), multiplied by the Seebeck coefficient (S) squared and the absolute temperature (T), over the thermal conductivity, which has both ionic (κ_l) and electronic (κ_{el}) contributions. The recent demonstration of $zT = 2.6$ in monocrystalline tin selenide [1] or $zT = 1.34$ in device form [2] has given a new breath to the field of thermoelectrics. By more than doubling the efficiency record for intrinsic bulk systems, SnSe has shown that economically competitive, nontoxic TE devices are within reach. The microscopic mechanism responsible for the performance is, however, not fully established, in particular due to sublimation effects in the high-T phase. Bulk SnSe is a narrow-band-gap semiconductor that undergoes a phase transition spanning the temperature range from 600 to 807 K, from a *Pnma* low-temperature phase as illustrated in Fig. 1 (space group 62) to a *Cmcm* high-temperature phase (space group 63) [3]. Both are distorted phases of rocksalt Fm3m (the isoelectronic structure of PbTe and SnTe). Exceptional values of zT are obtained for two main reasons: the intrinsically low thermal conductivity (in both phases) and the strong enhancement of the carrier concentration and conductivity in the *Cmcm* phase. This intricate interplay opens perspectives for many other layered or heterostructure materials, and calls for a profound understanding of the mechanisms. Properties can then be further engineered, e.g., by doping [2,4,5], nanostructuring [6–8], or strain [9,10]. Therefore, it is expected that any results we obtain from the physical comprehension of SnSe can be extrapolated to many other layered materials as SnTe and SnS (as in Ref. [11]).

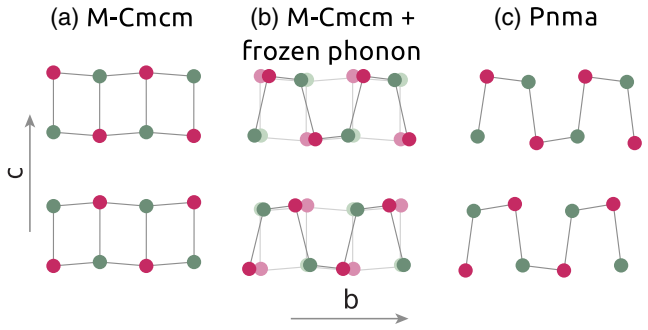

FIG. 1. Ball and stick model for both orthorhombic phases of SnSe. (a) Modified high-T *Cmcm* phase; (b) distortion of the modified *Cmcm* structure by the unstable phonon mode at Y, which leads to the stable *Pnma* phase; (c) low-T *Pnma* phase.

While many authors have described the different physical properties of this material, there is still an incomplete picture of the thermoelectric response of SnSe over the whole temperature range.

In this Letter, we offer a clear description of the experimental thermoelectric response of SnSe as a function of temperature. We perform advanced first-principles calculations to elucidate the origin of the increase in carrier concentration and the nature of the phase transition. Carrier concentrations are determined from intrinsic defect energies in the low- and high-T phases. We find that the calculated carrier concentration is dominated by Sn vacancies. Defect thermochemistry results, and carrier concentrations, show a strong dependence on both structure and temperature. We calculate Seebeck coefficients including the temperature dependence of the chemical potential, Fermi distribution, and the structure. Our results are in excellent agreement with experiments. We clarify the complex phase transition pathway between *Pnma* and *Cmcm*, and show that the high-T *Cmcm* phase is stabilized only when anharmonicity is included. Using harmonic phonon calculations and metadynamics simulations, we identify the sequence of elastic and phononic distortions which was suggested over 30 years ago by von Schnering and Wiedemeier [3]. The carrier concentrations are derived from intrinsic defect calculations within density functional theory. Perturbation theory is used for the harmonic phonon analysis [12], and the temperature dependent effective potential (TDEP) method [13], based on *ab initio* molecular dynamics, to calculate fully renormalized anharmonic effects and the complete P-T phase diagram. Metadynamics [14,15] allows us to explore the Born-Oppenheimer surface to refine our understanding of the phase transition. Seebeck coefficients are calculated from the Boltzmann transport equation within the constant relaxation time approximation [16]. Further details of the theoretical methods are given in the Supplemental Material [17].

We perform defect thermochemistry calculations to calculate defect formation energies E_d in the experimentally relevant Se rich limit. The results are shown in Fig. 2 vs the electron chemical potential μ_e for two experimental unit cells obtained at 790 (*Pnma*) and 829 K (*Cmcm*) [50], and where atomic positions are relaxed. The dominant defect in both phases is the Sn vacancy ($V_{\mathrm{Sn}}^{(2-)}$), which produces holes. The most striking difference between the two phases is that $V_{\mathrm{Sn}}^{(2-)}$ is strongly stabilized in *Cmcm* compared to *Pnma*.

Hall experiments by Zhao *et al.* [1] showed that the carrier concentration of SnSe varies strongly with T (Fig. 3). The first sign of a rapid increment in experimental electrical conductivity σ is at $T = 600$ K and continues steadily until 800 K. During the transition, the experimental concentration is well described by a single thermally activated level with energy barrier of 0.67 eV, shown as the magenta line in Fig. 3. Please note that in this small temperature interval, the $(1/T)$ behavior appears as a linear dependence on T, shown in Fig. 3. The magnitude of

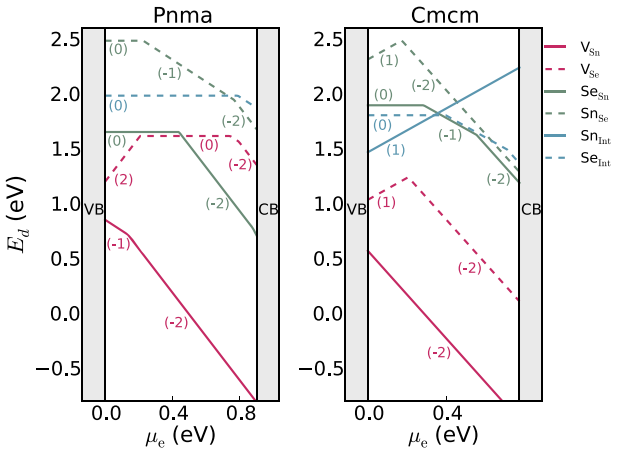

FIG. 2. The defect formation energies versus the electronic chemical potential μ_e are shown here for (a) the *Pnma* phase and for the (b) *Cmcm* phase in the Se rich limit. In both phases the most stable defects are the Sn vacancy, $V_{\mathrm{Sn}}^{(2-)}$ (intrinsic defect) which will produce holes. The slopes of E_d versus μ_e plots are the charges of the corresponding defects.

activation energy, 0.67 eV, is in good agreement with the calculated $\mathrm{Vac_{Sn}}$ formation energies at $\mu_e \simeq 0$ eV, Fig. 2, which strongly indicates that the increase in carrier concentration is due to creation of additional Sn vacancies during the phase transition. For temperatures below 600 K, the experimental concentration is constant for a sample that has been submitted to cycles of heating and cooling. In these conditions, the defects will be frozen into the structure with a constant carrier concentration.

Beyond a simple activated behavior, the defect formation energy will depend on temperature through μ_e, Fig. 2.

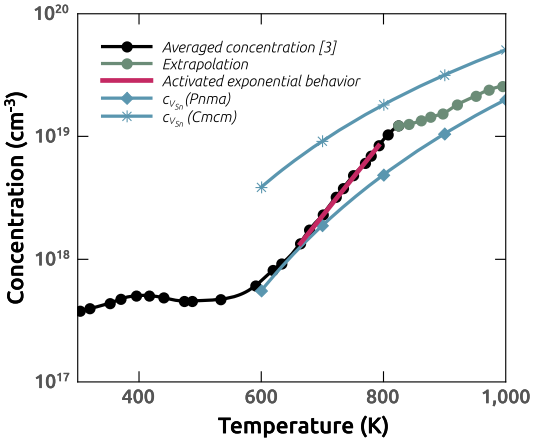

FIG. 3. Temperature dependence of the carrier concentration. In black, the average inverse Hall coefficient measured by Zhao *et al.* [1]. In green, the extrapolation determined as the carrier concentration which maximizes the Seebeck coefficient of the *Cmcm* phase (details in the Supplemental Material [17]). In blue, the carrier concentrations due to $V_{\mathrm{Sn}}^{(2-)}$ for the *Pnma* and *Cmcm* phases. In magenta, the simple thermally activated behavior, with a defect energy of 0.67 eV.

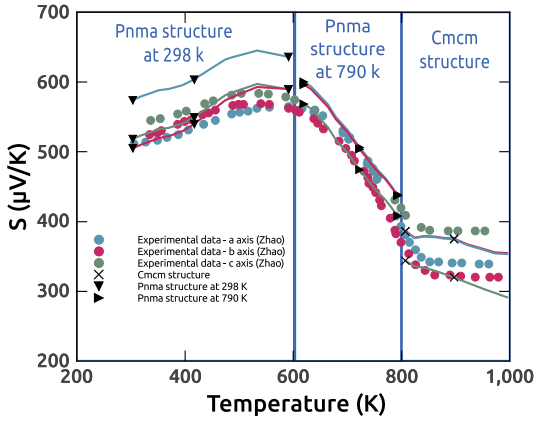

FIG. 4. Seebeck coefficients calculated with temperature-dependent carrier concentrations for three different regions of temperature. For the low-temperature region, we use the experimental structure of the *Pnma* phase at 298 K [50]. For the intermediate region, we used the *Pnma* experimental structure at 790 K [50]. For the last region, we used the *Cmcm* experimental structure at 825 K [50]. These calculations are compared with Ref. [1].

The temperature-dependent equilibrium concentration of defects, $c_{D^{(q)}}$, and corresponding carrier concentration, is calculated following Refs. [[51,52]], and summarized in the Supplemental Material [17]. In Fig. 3 we show the resulting calculated carrier concentrations for the *Pnma* and *Cmcm* phases alongside the experimental ones and its extrapolation for higher temperatures. Our predicted carrier concentration, essentially due to Sn vacancies, agrees with experiment above 600 K, suggesting the defects are equilibrated around this temperature. This also corresponds to the onset of the phase transition, which will affect defect mobilities. The model overestimates the carrier concentration somewhat in *Cmcm*, compared to our extrapolation of experiment. The slope is well reproduced, suggesting that above the phase transition the defect concentration is determined by thermodynamic equilibrium rather than being limited by mobility.

We calculate the Seebeck coefficients with the BOLTZTRAP code [16] which uses density functional theory (DFT) electronic band structures as input parameters (details in the Supplemental Material [17]). To take into account the temperature dependence of the carrier concentration, we adjust the chemical potential such that the doping level follows the experimental concentration and its extrapolation presented in Fig. 3. To account for the phase transition, we calculate the Seebeck coefficients for three different structures. The first two are *Pnma* structures at 295 and 790 K, and the third structure is *Cmcm* taken at 825 K. All cell parameters come from Ref. [50] and internal parameters are relaxed. The excellent agreement between experiment and theory in Fig. 4 was not present in previous publications [11,53,54]. We relate this level of agreement to both the variation of the carrier concentration and a correct representation of the phase transition.

The transition path between *Pnma* and *Cmcm* is subtle: the main differences are the b/a ratio and the degree of order and bond regularity. Our theoretically relaxed *Pnma* lattice constants, $a = 4.2095$, $b = 4.4968$, $c = 11.7201$ Å, slightly overestimate experimental ones [1,55] which is common in GGA DFT. Including dispersion forces does not affect the interlayer significantly (and is counterproductive with certain functionals); we do not use them in our results below. As temperature increases, there is a continuous phase transition towards the *Cmcm* phase, spreading over more than 200 K below the critical temperature of 807 K [3]. This transition can also be induced by pressure [56]. Our theoretically relaxed *Cmcm* lattice parameters are $a = 4.2838$, $b = 4.2816$, $c = 6.3250$ Å, which also compare well to experimental data [1].

The harmonic phonon band structure for *Pnma* is dynamically stable (see the Supplemental Material [17]) and compares well with experimental Raman and IR data at Γ [55], and theory in Ref. [57]. The harmonic phonon band structure for *Cmcm* (see the Supplemental Material [17]) presents a transverse optical phonon mode which is unstable at Γ along the directions to X and Y. Eigenvectors show that distortions appearing from the unstable phonon do not describe the full transition from *Cmcm* to *Pnma*: the phonon responsible for the transition must be a zone-boundary mode for the primitive cell of the *Cmcm* structure.

An experimental study of the phase transition [3] suggested that the transition is a two-step process, where, first, the atomic positions are shifted along the b axis continuously over a wide range of 200° below the transition temperature T_c and, second, the ratio of interplane cell constants changes from $b/a > 1$ to $b/a < 1$ over a range of 5 K near T_c. It is not clear that this last inversion of the cell parameters would lead to a first order structural transition. However, the recent experimental study of Zhao *et al.* [1] found a discontinuity at T_c in differential thermal analysis, confirming there are two steps in the transition.

Inspired by these results, we create a modified *Cmcm* structure where $b/a > 1$ by exchanging the values of a and b. Figure 5(a) shows the harmonic phonon bands of this structure with two unstable modes: one at the center of the Brillouin zone and a second at the zone boundary Y point. The unstable Γ point mode is ferroelectric, identical to the unstable mode of the unmodified *Cmcm* structure, and does not lead to *Pnma*. However, the Y point instability distorts the structure as in Fig. 1(b). Condensing this mode and relaxing leads to the low-temperature *Pnma* phase. This decomposition quantifies the two-step process of von Schnering: an elastic and a phononic distortion are combined to transform *Cmcm* to *Pnma*. This model explains numerous experimental results: in particular, the discontinuity in the differential thermal analysis originates in the elastic distortion, whereas the slow change of transport properties, starting 200 K before T_c, comes from the gradual phononic distortion.

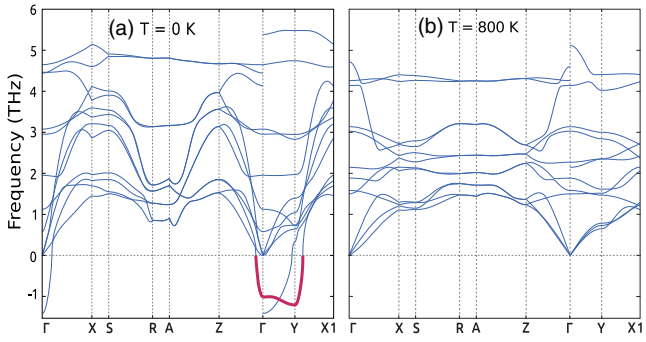

FIG. 5. Phonon band structure for SnSe in the *Cmcm* phase at different temperatures. (a) Harmonic 0 K phonons of the modified *Cmcm* structure where the *a* and *b* cell parameters are exchanged. A strong harmonic instability at the *Y* point returns the structure to the 0 K *Pnma* ground state. (b) Phonons of *Cmcm* calculated within TDEP at 807 K and for a pressure of 4 GPa—the structure is fully stabilized.

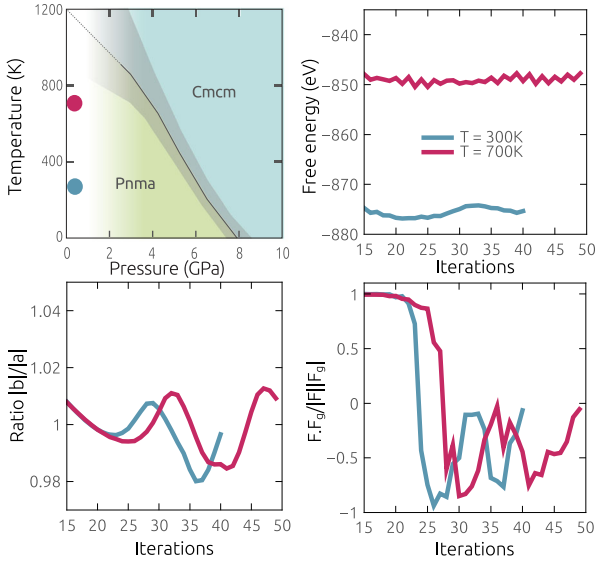

FIG. 6. Top left panel: full phase diagram of SnSe, from the TDEP method. The experimental T_c is recovered under a small volume contraction. Magenta and blue dots in the phase diagram: position in phase space for the metadynamics calculations. Top right panel: Gibbs free energy as a function of the metadynamics step, for 0.1 GPa at 300 and 700 K. Bottom left panel: b/a ratio of the crystal as a function of the metadynamics step. Bottom right panel: scalar product of the metadynamics and DFT generalized forces, indicating whether one is being pushed in to (> 1) or out of (< 1) a well in the PES.

In order to verify the possibility of a metastable *Cmcm* phase at ambient conditions, a metadynamics calculation was performed at 0.1 GPa and two different temperatures 300 and 700 K. This is a technique to map out the local potential energy surface (PES) by adding to the Born Oppenheimer potential a repulsive term which tracks the dynamics history [14,15,58,59]. Calculation details follow Ref. [60] (cf. the Supplemental Material [17]).

The evolution of the metadynamics for 300 and 700 K is shown in Fig. 6. The top right panel shows the Gibbs free energy, the bottom left the b/a ratio, and the bottom right panel the scalar product of two generalized forces on the unit cell, one coming from the PES and the other from the metadynamics Gaussians. A positive scalar product value indicates the metadynamics is moving into a well in the PES (initial phase), a negative value that it is climbing out, and a value near 0 that it is passing through saddle points between wells. The initial structure is *Pnma* for both temperatures. The first phase of the metadynamics is a slip of the SnSe bilayers, with rocksaltlike stacking. The dynamics then oscillates between $b/a > 1$ and $b/a < 1$. The principal conclusion is that both the layer slip and the oscillations observed do not show any metastable *Cmcm* phase, which validates our conclusions based on the harmonic phonons.

Our final step is to confirm the high-T stability of *Cmcm*. The phonon results above do not include the temperature dependence of the interatomic forces. In order to include full anharmonicity, we use the TDEP approach (details in the Supplemental Material [17]) [13]. Based on *ab initio* molecular dynamics in the canonical ensemble, an effective potential is fit to harmonic and anharmonic interatomic forces. The instability of *Cmcm* precludes the use of finite displacement methods as in Ref. [57]. With the TDEP method the force constants come from the full potential energy surface and contain infinite order renormalization of anharmonicities at the chosen temperature. This allows us to calculate the phonon band structure at finite temperature and the anharmonic free energies [26]. The top-left panel of Fig. 6 shows the pressure-temperature phase diagram of SnSe calculated from the Gibbs free energy within TDEP. We find that the relaxed GGA volume is slightly too large, and that the phase diagram is very sensitive to it. At low pressures only *Pnma* structures appear in the molecular dynamics: a small positive pressure is required to induce the phase transition to *Cmcm*. The "missing" pressure is probably linked to DFT shortcomings, such as a lack of accurate van der Waals contributions. The crystal structure is quite close to experiments, and we have tried all commonly available van der Waals functionals: none improve the results. Under a compression of around 4 GPa (volume change of 9%, faded zone in the figure), we obtain excellent agreement with experiment: the phase transition temperature of 807 K is reproduced, and the calculated phonon band structure of *Cmcm* is fully stabilized [Fig. 5(b)].

In summary, we present a complete account of the origin and evolution of the huge thermoelectric properties in SnSe. The fundamental driver is the order of magnitude increase of the carrier concentration, which we show is due to the energetics of charged defects in the two phases. Further, we decompose phonon and elastic instabilities to show that the transition from *Pnma* to *Cmcm* is indeed double, as suggested by von Schnering in 1981. There is a progressive change of bond angles over a range of 200 K,

and then a first order elastic transition at around 800 K, which inverts the b/a ratio. Finite temperature phonon calculations reconstruct the full phase diagram, and are necessary to stabilize *Cmcm*. The strong carrier-induced electrical conductivity can thus be engineered in chalcogenides [2,52] without destroying the thermopower as suggested by Hong *et al.* [61]. As the structures of SnSe are common in other materials classes, our analysis opens prospects for new layered and heterostructured thermoelectrics of unprecedented efficiency.

A. H. R. acknowledges the support of NSF 1434897 and the Donors of the American Chemical Society Petroleum Research Fund under Contract No. 54075-ND10. M. J. V. and A. D. acknowledge support from ULg, two Actions De Recherche Concertées (ACR) grants (TheMoTherm No. 10/15-03 and AIMED No. 15/19-09) from the Communauté Française de Belgique, support from COST networks EUSpec (MP1306) and XLIC (CM1204), and computer time from CECI, SEGI, and PRACE-3IP (EU FP7 Grant No. RI-312763) on Archer and Lindgren. Support from the Knut & Alice Wallenberg Foundation (KAW) project "Isotopic Control for Ultimate Material Properties" and the Swedish Foundation for Strategic Research (SSF) program SRL10-002 is gratefully acknowledged. Supercomputing resources were also provided by the Swedish National Infrastructure for Computing (SNIC).

[1] L.-D. Zhao, S.-H. Lo, Y. Zhang, H. Sun, G. Tan, C. Uher, C. Wolverton, V. P. Dravid, and M. G. Kanatzidis, Nature (London) **508**, 373 (2014).
[2] L.-D. Zhao *et al.*, Science **351**, 141 (2016).
[3] H. G. von Schnering and H. Wiedemeier, Z. Kristallogr. **156**, 143 (1981).
[4] J. Yang, G. Zhang, G. Yang, C. Wang, and Y. X. Wang, J. Alloys Compd. **644**, 615 (2015).
[5] E. K. Chere, Q. Zhang, K. Dahal, F. Cao, J. Mao, and Z. Ren, J. Mater. Chem. A **4**, 1848 (2016).
[6] F. Q. Wang, S. Zhang, J. Yu, and Q. Wang, Nanoscale **7**, 15962 (2015).
[7] Y.-M. Han, J. Zhao, M. Zhou, X.-X. Jiang, H.-Q. Leng, and L.-F. Li, J. Mater. Chem. A **3**, 4555 (2015).
[8] S. R. Popuri, M. Pollet, R. Decourt, F. D. Morrison, N. S. Bennett, and J. W. G. Bos, J. Mater. Chem. C **4**, 1685 (2016).
[9] S. H. Rhim, J.-H. Lee, and S. C. Hong, AIP Adv. **5**, 117147 (2015).
[10] D. D. Cuong, S. H. Rhim, J.-H. Lee, and S. C. Hong, AIP Adv. **5**, 117147 (2015).
[11] R. Guo, X. Wang, Y. Kuang, and B. Huang, Phys. Rev. B **92**, 115202 (2015).
[12] M. Verstraete and Z. Zanolli, in *Computing Solids: Models, Ab-initio Methods and Supercomputing, Lecture Notes of the 45th Spring School 2014*, edited by S. Blügel, N. Helbig, V. Meden, and D. Wortmann (Schriften des Forschungszentrums Jülich, 2014), Vol. 35, p. C2.
[13] O. Hellman, I. A. Abrikosov, and S. I. Simak, Phys. Rev. B **84**, 180301 (2011).
[14] R. Martoňák, Eur. Phys. J. B **79**, 241 (2011).
[15] R. Martoňák, A. Laio, M. Bernasconi, C. Ceriani, P. Raiteri, F. Zipoli, and M. Parrinello, Z. Kristallogr. **220**, 489 (2005).
[16] G. K. H. Madsen and D. J. Singh, Comput. Phys. Commun. **175**, 67 (2006).
[17] See Supplemental Material at http://link.aps.org/supplemental/10.1103/PhysRevLett.117.276601 for, which includes Refs. [16,19–50].
[18] X. Gonze *et al.*, Comput. Mater. Sci. **25**, 478 (2002).
[19] X. Gonze *et al.*, Z. Kristallogr. **220**, 558 (2005).
[20] H. J. Monkhorst and J. D. Pack, Phys. Rev. B **13**, 5188 (1976).
[21] Y. A. Timofeev, B. V. Vinogradov, and V. B. Begoulev, Phys. Solid State **39**, 207 (1997).
[22] S. Sassi, C. Candolfi, J.-B. Vaney, V. Ohorodniichuk, P. Masschelein, A. Dauscher, and B. Lenoir, Appl. Phys. Lett. **104**, 212105 (2014).
[23] P. Blaha, K. Schwarz, G. Madsen, D. Kvasnicka, and J. Luitz, *An Augmented Plane WaVe Plus Local Orbitals Program for Calculating Crystal Properties* (Vienna University of Technology, Austria, 2001), ISBN .
[24] E. Engel and S. H. Vosko, Phys. Rev. B **47**, 13164 (1993).
[25] A. H. Romero, E. K. U. Gross, M. J. Verstraete, and O. Hellman, Phys. Rev. B **91**, 214310 (2015).
[26] O. Hellman, P. Steneteg, I. A. Abrikosov, and S. I. Simak, Phys. Rev. B **87**, 104111 (2013).
[27] O. Hellman and I. A. Abrikosov, Phys. Rev. B **88**, 144301 (2013).
[28] P. E. Blöchl, Phys. Rev. B **50**, 17953 (1994).
[29] G. Kresse, Comput. Mater. Sci. **6**, 15 (1996).
[30] G. Kresse and D. Joubert, Phys. Rev. B **59**, 1758 (1999).
[31] G. Kresse and J. Furthmüller, Phys. Rev. B **54**, 11169 (1996).
[32] G. Kresse and J. Hafner, Phys. Rev. B **48**, 13115 (1993).
[33] J. P. Perdew, K. Burke, and M. Ernzerhof, Phys. Rev. Lett. **77**, 3865 (1996).
[34] S. Nosé, Molec. Phys. **52**, 255 (1984).
[35] W. G. Hoover, Phys. Rev. A **31**, 1695 (1985).
[36] P. Steneteg, O. Hellman, O. Y. Vekilova, N. Shulumba, F. Tasndi, and I. A. Abrikosov, Phys. Rev. B **87**, 094114 (2013).
[37] M. Omini and A. Sparavigna, Physica B: Condensed Matter **212**, 101 (1995).
[38] D. A. Broido, A. Ward, and N. Mingo, Phys. Rev. B **72**, 014308 (2005).
[39] S. Lee, K. Esfarjani, T. Luo, J. Zhou, Z. Tian, and G. Chen, Nat. Commun. **5**, 3525 (2014).
[40] R. Armiento and A. E. Mattsson, Phys. Rev. B **72**, 085108 (2005).
[41] A. E. Mattsson and R. Armiento, Phys. Rev. B **79**, 155101 (2009).
[42] R. Martoňák, A. Laio, and M. Parrinello, Phys. Rev. Lett. **90**, 075503 (2003).
[43] G. I. Csonka, J. P. Perdew, A. Ruzsinszky, P. H. Philipsen, S. Lebègue, J. Paier, O. A. Vydrov, and J. G. Ángyán, Phys. Rev. B **79**, 155107 (2009).
[44] S. Nosé, J. Chem. Phys. **81**, 511 (1984).
[45] S. Nosé, Prog. Theor. Phys. **103**, 1 (1991).

[46] D. M. Bylander and L. Kleinman, Phys. Rev. B **46**, 13756 (1992).
[47] C. G. Van de Walle and J. Neugebauer, J. Appl. Phys. **95**, 3851 (2004).
[48] G. Makov and M. C. Payne, Phys. Rev. B **51**, 4014 (1995).
[49] P. B. Allen, Phys. Rev. B **17**, 3725 (1978).
[50] T. Chattopadhyay, J. Pannetier, and H. V. Schnering, J. Phys. Chem. Solids **47**, 879 (1986).
[51] C. Bera, S. Jacob, I. Opahle, N. S. H. Gunda, R. Chmielowski, G. Dennler, and G. K. H. Madsen, Phys. Chem. Chem. Phys. **16**, 19894 (2014).
[52] S. Bhattacharya, N. S. H. Gunda, R. Stern, S. Jacobs, R. Chmielowski, G. Dennler, and G. K. H. Madsen, Phys. Chem. Chem. Phys. **17**, 9161 (2015).
[53] G. Shi and E. Kioupakis, J. Appl. Phys. **117**, 065103 (2015).
[54] X. Guan, P. Lu, L. Wu, L. Han, G. Liu, Y. Song, and S. Wang, J. Alloys Compd. **643**, 116 (2015).
[55] H. Chandrasekhar, R. Humphreys, U. Zwick, and M. Cardona, Phys. Rev. B **15**, 2177 (1977).
[56] S. Alptekin, J. Mol. Model. **17**, 2989 (2011).
[57] J. Carrete, N. Mingo, and S. Curtarolo, Appl. Phys. Lett. **105**, 101907 (2014).
[58] A. Laio and F. L. Gervasio, Rep. Prog. Phys. **71**, 126601 (2008).
[59] A. Laio and M. Parrinello, in *Computer Simulations in Condensed Matter Systems: From Materials to Chemical Biology* (Springer, New York, 2006), Vol. 1, p. 315.
[60] R. Martoňák, D. Donadio, A. R. Oganov, and M. Parrinello, Nat. Mater. **5**, 623 (2006).
[61] A. J. Hong, L. Li, H. X. Zhu, Z. B. Yan, J.-M. Liu, and Z. F. Ren, J. Mater. Chem. A **3**, 13365 (2015).